Nanoscale

Accepted Manuscript

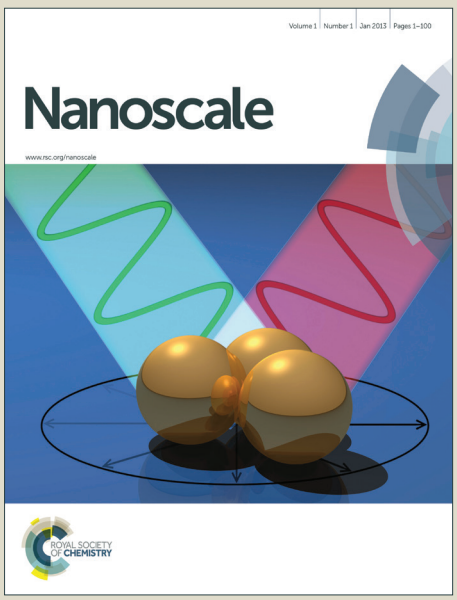

ROYAL SOCIETY OF CHEMISTRY

www.rsc.org/nanoscale

Nanoscale

RSCPublishing

COMMUNICATION

Gradual-order enhanced stability: Frozen section of electrospun nanofibers for energy storage

Cite this: DOI: 10.1039/xoxxoooooox

Xinlei Ma,[a] Mianqi Xue,[*b,d] Fengwang Li,[c] Jitao Chen,[*c] Dong Chen,[b] Xusheng Wang,[c] Feng Pan[d] and G. F. Chen[b]

Received ooth January 2012,
Accepted ooth January 2012

DOI: 10.1039/xoxxoooooox

www.rsc.org/

The combination of the electrospinning and frozen section has been used to lower the scale of the active materials gradually, thus avoiding the nano-reunion effectively to a certain extent in the electrode fabrication. The as-fabricated electrode-based supercapacitor possesses high electrochemical capacitance and good stability. The results demonstrate a universal top-down route for controllable fabrication of homodisperse nanoparticle electrodes for high performance electrochemical devices.

Introduction

As energy storage devices, supercapacitors have been attracting intensive attention owing to their unique advantages including high power electrical energy storage, long cycle life and superior reversibility, which currently provide a bridge between batteries and conventional electrostatic capacitors (dielectric or electrolytic capacitors)[1-8]. In this field, the main challenge remains to develop their energy density closed to the current rechargeable battery, while maintaining their inherent stability.[1,6] Materials with pseudocapacitance such as transition-metal oxides (ruthenium oxide[9], iron oxide[10], nickel hydroxide[11], manganese oxide[12,13] etc.) and conducting polymers (polyanilines[14], polypyrroles[15], polythiophenes[16] etc.) possess the possibility to satisfy the demanding of energy density but are limited by the poor cycle life for practical applications. In this sense, improving the stability of pseudocapacitance-based supercapacitors while maintaining high capacity is the alternative solution for the next generation supercapacitors.

Several creative methods, especially nanofabrication of active materials[17-20], have been developed for enhancing the stability of pseudocapacitance-based devices. Normally, developments of the nanotechnologies are improving the scale of the active materials for energy storages down to 50 nm, which can enhance the utilization of active materials significantly and shorten the transport path of ions and electrons, leading to higher electrochemical performances.

For example, template-free solution method combined with a post annealing treatment was developed to synthesize interconnected mesoporous nanosheets for supercapacitors[17]; hydrothermal treatment was reported to fabricate 3D graphene and polypyrrole based hydrogel for supercapacitors[18]; controllable in-situ electrochemical growth was used to produce conducting polymer nanowires on the graphene patterns for microsupercapacitor[19]. Such novel methods have successfully fabricated nano electrode materials which exhibited ultrahigh specific capacitance and excellent cycling stability. However, they are still limited on mass production and unconsistency for the inherent agglomeration of nanoparticles.

Along with the development of technical level, electrospinning is widely used in energy industry in last few years for its simplicity, scale controllability, low cost and especially its increasing production rate[21]. Recently, we developed a modified electrospinning method for fabricating flexible micro-supercapacitor with sub-10-nm-scale MnO_2 nanoparticles[22]. This method can easily produce MnO_2 nanoparticles, which exhibited outstanding electrochemical performances for the micro-supercapacitor with high specific capacitance and good stable cycle. The enhancements were mainly due to the nanometer size effect and the microminiaturization of the devices. Nonetheless, when amplifying the devices to the regular size, the inherent agglomeration of the nanoparticles mentioned-above still release their negative impact on the electrochemical performances of the supercapacitors. Here we improved this procedure to generate homodispersed nanoparticle electrodes for supercapacitors in two steps: First, electrospin parallel nanofibers with precursor of active material on paraffin substrates, and then cut them via frozen section to control the final morphology of the active materials. The specific capacitance of the final nanomaterial after calcination and ultrasonic can reach as high as 420 F g^{-1} at a discharge current density of 0.1 A g^{-1} which is at the same level as the highest specific capacitance in other reported

MnO_2 composites. On this basis the most prominent electrochemical performance is the stability of this nanomaterial, which is far beyond that of nanomaterial without frozen section (after 4000 consecutive cycles, this nanomaterial retained more than 92 % of its initial capacitance, while nanomaterial without frozen section decreased quickly to 80 % after less than 3000 cycles).

Experimental section

Synthesis of FS-MnO_2 nanoparticles: 0.7 g manganese acetate was dissolved in 4 mL water, and then mixed with 10 mL PVP (10 wt %). The mixture was vigorously stirred at 50 ℃ for 5 h to obtain viscous sol suitable for electrospinning. The solution was then immediately loaded into a plastic syringe equipped with a fine capillary metallic needle. The needle was connected to a high-voltage supply that generated a DC voltage of 10 kV. A piece of paraffin substrate with two grounded good parallel electrodes was placed around 7 cm below the tip of the needle to collect the aligned nanofibers. The flow rate of the solution was maintained at 0.5 mL h^{-1}. The electrospinning process was conducted in air at room temperature. The as-fabricated paraffin substrate with aligned nanofibers on the surface was then cut by frozen section. In the cutting step, the blade was parallel to gold electrodes. After this, the isometric nanowires with MnO_2 precursors was heated up (first 150 ℃ for 2 h and then 500 ℃ for 3 h) to remove the paraffin and then calcined to MnO_2 in a nitrogen atmosphere.

Electrochemical measurements: After annealing, the oxides were mixed with 10 wt % carbon black and 5 wt % PTFE and ground to form a paste. Then the paste was rolled into uniform sheets with thicknesses around 40 μm, and finally punched into electrodes. A two-electrode cell configuration was used to measure the performance of supercapacitor in 1 M Na_2SO_4 aqueous electrolytes. Cyclic voltammetry and galvanostatic charge/discharge tests were used to characterize the electrochemical performances of the supercapacitor devices. The cyclic voltammetry curves were scanned from 0 to 0.95 V in 1 M Na_2SO_4 at different scan rates, and the charge/discharge processes were performed by cycling the potential from 0 to 1 V at different current densities. The cyclic stabilities were characterized using galvanostatic charge/discharge experiments with a constant current density of 1 A g^{-1} for over 4,000 cycles.

Results and discussion

Figure 1 depicts the procedure used to fabricate MnO_2 micrometer-long nanofiber arrays, which is based on the electrospinning and frozen section. Firstly, a flexible polydimethylsiloxane (PDMS) substrate was separated from a silica wafer and then one paraffin substrate was molded from as-fabricated PDMS stamp, as shown in Figure 1a. Then the paraffin substrate was used as collector in the next electrospinning step. Figure 1b schematically illustrates the apparatus used to prepare the parallel nanofibers with MnO_2 precursors by electrospinning. The solution used for the electrospinning was a mixture of poly(vinylpyrrolidone) (PVP) and manganese acetate. The orderliness of electrospun fibers was controlled by using two parallel electrodes which have been sputtered on the surface of paraffin substrate. The as-fabricated parallel nanofibers were then cut into microribbons, which are composed of parallel isometric nanowires (micrometer in length) via frozen section. In the cutting step, the blade was perpendicular to nanofibers, as shown in Figure 1c. After that, the isometric nanowires with MnO_2 precursors was heated up to remove the paraffin and then calcined to MnO_2.

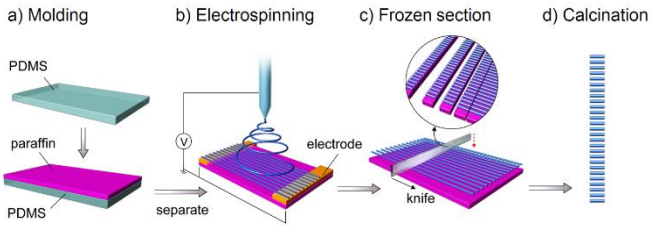

Figure 1. A schematic illustration of the procedure used to fabricate MnO_2 micro-length nanofiber arrays. (a) Preparation of paraffin substrate via molding form PDMS substrate. (b) Fabrication of the parallel nanofibers with MnO_2 precursors on the paraffin substrate by electrospinning. (c) Cut the nanofibers to isometric nanowires through the frozen section. (d) Heat to remove the paraffin and then pyrolyzed the MnO_2 precursors in the isometric nanowires to MnO_2.

In our previous work[22], the orderliness of electrospun fibers was verified to have a significant effect on the performance of energy devices which can ensure the conductivity of ions and electrons. **Figure 2**a and b show the SEM image of aligned electrospun nanofibers. In the electrospinning step, manganese source solution was loaded into a plastic syringe equipped with a gauge needle made of stainless steel. The needle was connected to the syringe through a silicone tube. A high voltage was applied on the needle by a direct current power supply. The flow rate of the solution was controlled by a syringe pump. Aligned nanofibers were collected on a paraffin substrate with two grounded parallel electrodes. As shown in these figures, the electrospun fibers are aligned on the substrate. The insulating gap between two grounded electrodes alters the configuration of electrostatic forces acting on the nanofibers spanning across the gap. As shown in figure 2a, the fibers are randomly oriented out of the region of insulating gap and well aligned between two electrodes. The as-fabricated parallel nanofibers were then cut into isometric nanowires through the frozen section. Figure 2c shows the isometric nanowires after frozen section on a silica substrate.

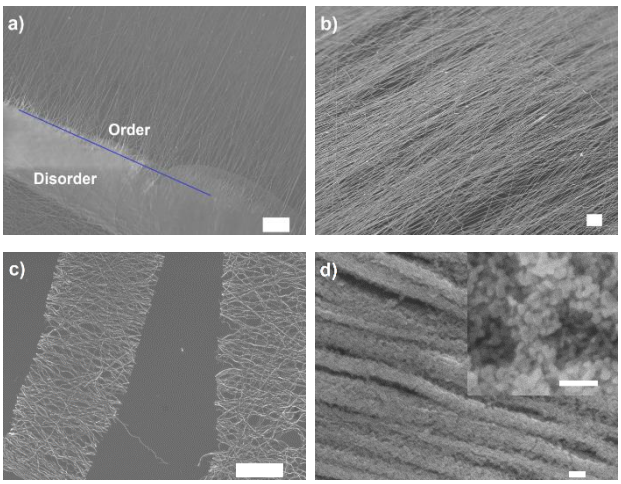

Figure 2. The resulting nanofibers in different stages. (a, b) Aligned nanofibers via electrospinning on the paraffin substrate with two ground electrodes. (c) Isometric nanowires after frozen section on a silica substrate after remove paraffin. (d) Nanowires with MnO_2 nanoparticles after calcination. Inset is the magnified view of the MnO_2 nanoparticles. Scale bars: (a-c) 10 μm, (d) 100 nm.

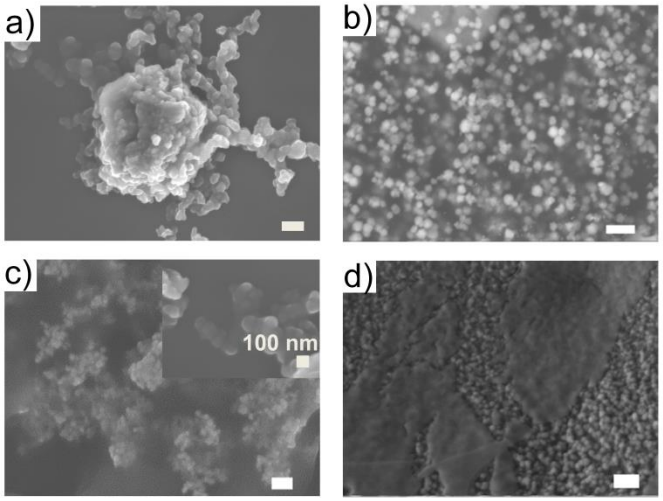

Figure 3. The topographic images of the calcined electrospun nanofibers after ultrasonic treatments with or without frozen section and their based electrodes. (a) The irregular aggregations of MnO_2 nanoparticles after ultrasonic treatments of the electrospinning nanofibers without frozen section. (b) The monodisperse MnO_2 nanoparticles after ultrasonic treatments of the electrospinning nanofibers with frozen section. The topographic images of the electrodes corresponding to the irregular aggregations of MnO_2 nanoparticles (c and the insert) and the topographic image of the electrodes corresponding to the uniform MnO_2 nanoparticles (d). Scale bars: (a) 500 nm, (b) 100 nm, (c) 1 μm, (d) 100 nm.

Afterwards, the isometric nanowires with MnO_2 precursors were heated up to remove the paraffin and then pyrolyzed to MnO_2 in a nitrogen atmosphere. The carbon content after calcination at 500 ℃ is 4.3%. Figure 2d shows the final nanowires composed of MnO_2 nanoparticle. Inset is the magnified view of the MnO_2 nanoparticles. After annealing, the oxides were mixed with 10 wt % carbon black and 5 wt % PTFE and ground to form a paste. Then the paste was rolled into uniform sheets with thicknesses around 40 μm, and finally punched into electrodes. We have tried different component ratio of oxides, carbon black and PTFE, such as 80/15/5 and 70/20/10. The increased ratio of carbon black can't decrease the aggregation of nanoparticles; the abundant carbon black improves the conductivity and lowers the ratio of inert component. For the choice of the component ratio around 85/10/5, the electrode can load more electroactive material and increase the volumetric energy density of the supercapacitor.

Afterwards, we investigated the difference in the electrodes formation procedure of calcined electrospun nanofibers with or without frozen section. **Figure 3**a shows the irregular aggregations of MnO_2 nanoparticles after ultrasonic treatments of the electrospinning nanofibers without frozen section. Cutting the nanowire into isometric nanowires not only enables the nanowires get smaller and isolate from each other but also get smashed easier by sonication, which will reduce the aggregation(as shown in 3a) greatly. Besides, the introducing of paraffin in the frozen section can wets nanowires while heating and fill among them. With the increase of temperature, the paraffin gets decomposition/gasification which prevents the nanoparticles from aggregating. The electrospinning nanofibers after frozen section, on the other hand, could form monodisperse nanoparticles after ultrasonic treatments (referred as FS-MnO_2), as shown in Figure 3b. Figure 3c and 3d show the topographic images of the electrodes consisting of electrospun-nanofiber-based composite material (corresponding to Figure 3a and 3b), acetylene black and binder. A rough surface with obvious large nanoparticle aggregates can be observed corresponding to the irregular aggregations of MnO_2 nanoparticles shown in Figure 3a, when the flat surface corresponding to the uniform MnO_2 nanoparticles shown in Figure 3b.

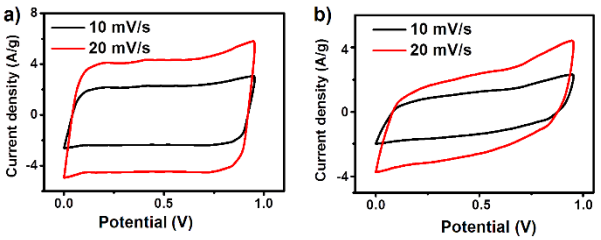

Figure 4. Comparison of CVs scanned from 0 to 0.95 V in 1 M Na_2SO_4 (aq) for the FS-MnO_2 electrodes (a) and MnO_2 electrodes (b) at scan rates of 10 and 20 mV s^{-1}.

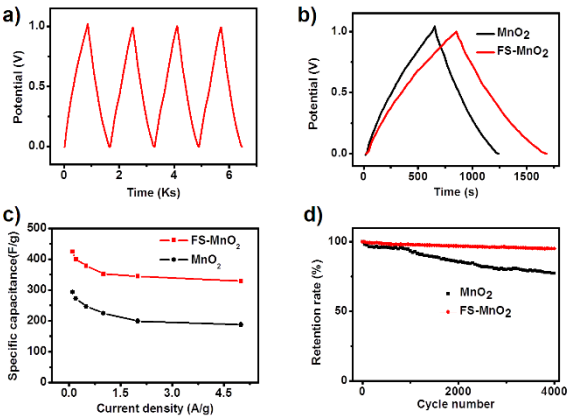

Figure 5. Electrochemical performances. (a, b) Charge-discharge (voltage versus time) curves at a current density of 0.5 A g^{-1}. (c) Specific capacitance of MnO_2 and FS-MnO_2 at difference charge/discharge current densities. (d) Cycle stability of the MnO_2 and FS-MnO_2 based supercapacitors at 1 A g^{-1}. The high voltage of the test is 1 V.

Figure 4 shows representative cyclic voltammograms (CVs) for the FS-MnO_2 electrode (Figure 4a) and MnO_2 electrode (Figure 4b) at the scan rates of 10 and 20 mV s^{-1} in 1 M Na_2SO_4 recorded in the potential range of 0 to 0.95 V, respectively. All voltammetric curves exhibit a nearly symmetrical rectangular shape, while the curves of MnO_2 electrode present a slight deviation from rectangular shape (as shown in Figure 4b). These voltammograms show the typical behavior of supercapacitors, indicatives a more ideal capacitor behavior based on FS-MnO_2 than that based on MnO_2 nanoparticles without frozen section. Comparing the four curves, there is a clearer symmetry and rectangular shape in the FS-MnO_2, especially at high scan rates, which indicates the charge transfer at the interface between MnO_2 and electrolyte and ion-diffusion rates in the FS-MnO_2 electrode are faster than that in the MnO_2 electrode.

To further study the electrochemical performances of FS-MnO_2, these electrodes were fully characterized by galvanostatic charge/discharge and cycling-life measurement. **Figure 5**a presents the galvanostatic charge/discharge curves of FS-MnO_2 at a current density of 0.5 A g^{-1}, and these were close to a triangular shape and all of the charging curves are symmetrical with their corresponding discharge counterparts as well as their good linear voltage time

profiles, confirming the high columbic efficiency, excellent reversibility, and good charge propagation across the electrode. Galvanostatic charge–discharge curves shown in Figure 5b reveal that the FS-MnO_2 electrode materials can provide a larger specific capacitance around 400 F g^{-1} than the MnO_2 without frozen section. The specific capacitances are calculated according to $C_m = I/[(\Delta V/\Delta t)m]$, where C_m is the specific capacitance (F g^{-1}), I is the charge/discharge current, ΔV is 1 V, m is the mass of the active materials (g). Figure 5c shows the specific capacitance values of two different MnO_2 electrodes at different current densities. FS-MnO_2-based supercapacitor not only exhibits high specific capacitance values but also maintains them well at high current density compared with MnO_2-based supercapacitor, which indicates the higher power density of FS-MnO_2 and better high-rate charge/discharge characteristics. The FS-MnO_2 not only facilitates the cation diffusion between electrolyte and electrode but also is beneficial to overcome the poor electrical conductivity of MnO_2, which would enhance the electrochemical performance of the supercapacitor. Another advantage of this type of FS-MnO_2-based supercapacitor is the good stability, as shown in Figure 5d, less than 10 % loss of the capacitance has been observed after 4000 cycles at 1 A g^{-1}.

Compared with our previous report about electrospun MnO_2 nanoparticles-based micro-supercapacitor[22], the specific capacitance of the electrospun MnO_2 nanoparticles is reduced from ~350 F/g down to below 300 F/g when used in conventional supercapacitor. This result is mainly caused by the irregular aggregations of MnO_2 nanoparticles. In the design of micro-supercapacitor, the active materials are in-situ electrospun as electrodes and the thickness of the electrode is controlled in a micrometer level. However, in the fabrication of conventional supercapacitor, it must be spread for preparation of electrodes. The aggregations of MnO_2 nanoparticles will generate in this procedure for the natural limitations of nanoparticles. These aggregations cause the increase of inert components of active material, leading to the reduction of both charge transfer and ion-diffusion rates. The adverse effects directly result in lower and worse-maintained specific capacitance, also stable cycle life, in the conventional supercapacitor than the micro-supercapacitor.

On the other hand, the results show that using frozen section on electrospun nanofibers for fabricating homodisperse MnO_2 nanoparticles exhibits the possibility to solve these problems. The FS-MnO_2 based supercapacitor shows higher specific capacitance and better stability than the MnO_2 (without frozen section) based supercapacitor. The high performance of the FS-MnO_2 based supercapacitor (high and well-maintained specific capacitance, stable cycle life) in our design is mainly due to the uniform dispersing in the electrodes. For this improvement, the 10 nm scale nanoparticles and their uniform blending with conductive additive ensure the short paths of ion diffusion in the nanoparticles and good electron conductivity. Furthermore, the homodisperse can well confine the ionic resistance for little proportion of inert components whose redundancy shortens the diffusion path. Additionally, the residual carbon after calcination of electrospun aligned nanofibers can further enhance the electron transport ability. Therefore, the nanomaterial can be better utilized in the FS-MnO_2 based supercapacitor, showing high electrochemical performances.

Conclusions

In summary, a low-cost and eco-friendly approach was used to fabricate high-performances supercapacitor with nanoparticle-homodispersed electrodes. The as-fabricated supercapacitor possesses electrochemical capacitance as high as 420 F g^{-1} at a discharge current density of 0.1 A g^{-1}, as well as good stability, retaining more than 92 % of its initial capacitance after 4000 consecutive cycles. The results demonstrates that the combination of the electrospinning and frozen section can lower the scale of the active materials gradually, avoiding the nano-reunion effectively in the electrode fabrication. It's also worth pointing out that the technique we describe here is a universal method, which can be applied on other function materials to form controllable nanostructures, not just electrochemical active materials.

The authors wish to thank Y. Duan, R. Li, L. Jiang, X. Wang for their fruitful discussions and helpful comments. This work was supported by the Natural Science Foundation of China (21304002), Qinghai Province Science and Technology program (2012-G-Y28, 2013-G-Q12A-1) and Shenzhen Science and Technology Innovation Commission (ZDSY20130331145131323, XZZ20120829172325895, JCYJ20120614150338154, SGLH20120928095706623, JCYJ2012 0829170028561).

Notes and references

[a]*Research Center for Bioengineering and Sensing Technology, University of Science & Technology Beijing, Beijing, P. R. China*
[b]*Institute of Physics and Beijing National Laboratory for Condensed Matter Physics, Chinese Academy of Sciences, Beijing 100190, China. E-mail: xuemq@iphy.ac.cn*
[c]*Beijing National Laboratory for Molecular Sciences, College of Chemistry and Molecular Engineering, Peking University, Beijing 100871, China. E-mail: chenjitao@pku.edu.cn*
[d]*School of Advanced Materials, Peking University, Peking University Shenzhen Graduate School, Shenzhen 518055, China*

† Electronic Supplementary Information (ESI) available: [Detailed information about experimental methods]. See DOI: 10.1039/b000000x/

1. J. Chmiola, C. Largeot, P. L. Taberna, P. Simon, Y. Gogotsi, *Science* **2010**, *328*, 480.
2. V. Singh, D. Joung, L. Zhai, S. Das, S. I. Khondaker, S. Seal, *Prog. Mater. Sci.* **2011**, *56*, 1178.
3. M. F. El-Kady, V. Strong, S. Dubin, R. B. Kaner, *Science* **2012**, *335*, 1326.
4. W. Gao, N. Singh, L. Song, Z. Liu, A. L. M. Reddy, L. Ci, R. Vajtai, Q. Zhang, B. Wei, P. M. Ajayan, *Nat. Nanotech.* **2011**, *6*, 496.
5. W. Chen, R. B. Rakhi, L. Hu, X. Xie, Y. Cui, H. N. Alshareef , *Nano Lett.* **2011**, *11*, 5165.
6. D. Pech, M. Brunet, H. Durou, P. Huang, V. Mochalin, Y. Gogotsi, P.-L. Taberna, P. Simon, *Nat. Nanotech.* **2010**, *5*, 651.
7. H. B. Li, M. H. Yu, F. X. Wang, P. Liu, Y. Liang, J. Xiao, C. X. Wang, Y. X. Tong, G. W. Yang, *Nat. Commun.* **2013**, *4*, 1894.
8. M. F. El-Kady, R. B. Kaner, *Nat. Commun.* **2013**, *4*, 1475.
9. J. S. Ye, H. F. Cui, X. Liu, T. M. Lim, W. D. Zhang, F. S. Sheu, *Small* **2005**, *1*, 560.
10. Q. Qu, S. Yang, X. Feng, *Adv. Mater.* **2011**, *23*, 5574.
11. H. Jiang, T. Zhao, C. Li, J. Ma, *J. Mater. Chem.* **2011**, *21*, 3818.
12. W. Wei, X. Cui, W. Chen, D. G. Ivey, *Chem. Soc. Rev.* **2011**, *40*, 1697.
13. X. Lang, A. Hirata, T. Fujita, M. Chen, *Nat. Nanotech.* **2011**, *6*, 232.
14. K. Zhang, L. L. Zhang, X. S. Zhao, J. Wu, *Chem. Mater.* **2010**, *22*, 1392.
15. S. Biswas, L. T. Drzal, *Chem. Mater.* **2010**, *22*, 5667.
16. A. Laforgue, P. Simon, C. Sarrazin, J. F. Fauvarque, *J. Power Sour.* **1999**, *80*, 142.
17. G. Zhang, X. W. Lou, *Adv. Mater.* **2013**, *25*, 976.

18. Y. Zhao, J. Liu, Y. Hu, H. Cheng, C. Hu, C Jiang, L. Jiang, A. Cao, L. Qu, *Adv. Mater*. **2013**, *25*, 591.
19. M. Xue, F. Li, J. Zhu, H. Song, M. Zhang, T. Cao, *Adv. Funct. Mater.* **2012**, *22*, 1284.
20. A. S. Aricò, P. Bruce, B. Scrosati, J. M. Tarascon, W. Schalkwijk, *Nat. Mater.* **2005**, *4*, 366.
21. V. Thavasi, G. Singh, S. Ramakrishna, *Energy Environ. Sci*. **2008**, *1*, 205.
22. M. Xue, Z. Xie, L. Zhang, X. Ma, X. Wu, Y. Guo, W. Song, Z. Li, T. Cao, *Nanoscale* **2011**, *3*, 2703.